PERGAMON

International Journal of Heat and Mass Transfer 42 (1999) 4093–4106

International Journal of HEAT and MASS TRANSFER

www.elsevier.com/locate/ijhmt

Heat transfer and fluid flow of natural convection around large horizontal cylinders

K. Kitamura [a,*], F. Kami-iwa [a], T. Misumi [b]

[a] Department of Mechanical Engineering, Toyohashi University of Technology, Tempaku-cho, Toyohashi 441-8580, Japan
[b] Department of Mechanical Engineering, Kagoshima National College of Technology, Hayato-cho, Kagoshima 899-5102, Japan

Received 26 July 1998; received in revised form 24 February 1999

Abstract

Natural convective flows of water around large horizontal cylinders were investigated experimentally. The main concerns were the turbulent transition and its influence on the local heat transfer. The cylinders were heated with uniform heat flux and their diameters were varied from 60 to 800 mm to enable experiments over a wide range of modified Rayleigh numbers, $Ra^*_D = 3.0 \times 10^8$ to 3.6×10^{13}. The flow fields around the cylinders and the surface temperatures of the cylinders were visualized to investigate the turbulent transition mechanisms. The results show that three-dimensional flow separations occur first at the trailing edge of the cylinder when Ra^*_D beyond 2.1×10^9, and the separation points shift upstream with increasing the Rayleigh numbers. These separations become a trigger to the turbulent transition. Transitional and turbulent flows appear downstream of the separations at higher Rayleigh numbers. However, they occupy a relatively small portion of the cylinder surfaces even at the maximum Rayleigh numbers of the present experiments. The local heat transfer coefficients were also measured. The results show that the coefficients are increased markedly in the transitional and turbulent regions.

1. Introduction

Natural convective flows around heated, horizontal cylinders are encountered in many technological applications. These applications have motivated a considerable body of research on their flow and heat transfer characteristics. However, main concerns of previous studies have been directed to laminar natural convection, while relatively less attention has been paid to turbulent natural convection. This is partly because turbulent flows are realized only around the large cylinders, and the experiments using such cylinders are difficult to perform in a limited laboratory framework. The lack of experimental data has also hampered the analytical studies on turbulent natural convection around cylinders.

Despite these circumstances, several workers have carried out the experiments on the turbulent natural convection. However, most of them have measured overall heat transfer coefficients from the isothermal cylinders. Summarizing these data, several sets of empirical or semi-empirical correlation equations have been proposed, for example, by McAdams [1], Morgan [2], Churchill and Chu [3] and others. These equations are generally expressed as:

$$Nu_m = C\,Ra_D^n \tag{1}$$

C and n in Eq. (1) stands for the proportional constant and the exponent, which are determined empirically from the heat transfer data. Although the proportional constant C differs slightly between the workers, the

* Corresponding author.

0017-9310/99/$ - see front matter
PII: S0017-9310(99)00079-4

Nomenclature

D	diameter of cylinder
g	gravitational acceleration
h_m	overall heat transfer coefficient, $q_w/(T_{wm}-T_\infty)$
h_θ	local heat transfer coefficient, $q_w/(T_{w\theta}-T_\infty)$
Nu_m	average Nusselt number, $h_m D/\lambda_{fm}$
Nu_θ	local Nusselt number, $h_\theta D/\lambda_{f\theta}$
P	averaged axial pitch of separation
Pr	Prandtl number
q_w	wall heat flux
Ra_D	Rayleigh number, $g\beta(T_w-T_\infty)D^3/(\alpha\nu)_{fm}$
Ra_D^*	modified Rayleigh number, $g\beta q_w D^4/(\lambda\alpha\nu)_{fm}$
T	temperature
T_{wm}	average wall temperature
$T_{w\theta}$	local wall temperature at location θ

Greek symbols

α	thermal diffusivity of fluid
β	coefficient of volume expansion
λ	thermal conductivity of fluid
θ	angle from cylinder bottom
ν	kinematic viscosity of fluid

Subscripts

c	critical
fm	at average film temperature
fθ	at local film temperature
m	average
w	wall
θ	at angular location θ
∞	at ambient

exponent $n = 1/3$ is adopted consistently for the turbulent heat transfer. The workers have also proposed the correlating equations for the laminar heat transfer with the same form as Eq. (1), where the exponent $n = 1/4$ is commonly used instead of $n = 1/3$. Moreover, based on these results, they have also obtained the critical Rayleigh numbers for the turbulent transition, Ra_{DC}. The critical numbers were defined as the Rayleigh numbers corresponding to the deflection points from $n = 1/4$ to $1/3$ in log Nu_m–log Ra_D plane. However, the numbers show large discrepancies between the workers: For example, $Ra_{DC} = 10^9$ was obtained by McAdams [1], while $Ra_{DC} = 10^7$ by Morgan [2]. Thus, we have been unable to determine the critical Rayleigh numbers exactly from these results. Besides, the results on the overall heat transfer will not provide the basic insight into the flow and temperature fields around the cylinders.

To the best of present authors' knowledge, the following two studies have investigated the flow and temperature fields of the turbulent natural convection over heated cylinders. One is the analytical work by Farouk and Guceri [4] and another is the experimental work by Hattori [5]. Farouk and Guceri have first applied a k–ε model to the turbulent natural convection of air, and have calculated time-averaged velocities, temperatures, vorticities and turbulent kinetic energies around the cylinders in the Rayleigh number range from 5×10^7 to 5×10^{10}. They employed similar models and empirical constants as those for the turbulent forced convection. However, their results show considerable differences from the experimental results by Hattori [5], particularly in the local Nusselt numbers and on the conditions of turbulent transition. Thus, further improvement of the models and empirical constants will be necessary on their analysis.

Meanwhile, Hattori [5] has measured the time-averaged velocities and the turbulent quantities such as Reynolds shear stresses $-\overline{u'v'}$ and turbulent heat fluxes $-\overline{u't'}$ within the turbulent boundary layers of air. Although the measurements have been performed at limited locations over a cylinder in the narrow range of Rayleigh numbers from 3×10^9 to 3×10^{10}, the results will provide basic knowledge on the turbulent transport and will become a database for turbulence modeling.

Despite the contributions of these studies, several subjects remain unsolved. One of such subjects is related with a turbulent transition. We suppose a case where the heated cylinder is placed horizontally in a quiescent fluid as shown in Fig. 1. When the diameter of the cylinder is small, the buoyant flow induced around the cylinder will become laminar throughout the surface as shown in Fig. 1(a). The flow will become gradually unstable when the cylinder diameter is increased, and a transition to turbulence will finally occur over the cylinders as is schematically illustrated in Fig. 1(b). However, it has been still uncertain where and how the turbulent transition occurs over the cylinders, and what kind of parameters affects the transition. Another subject to be clarified is the process from the beginning of transition to the fully developed turbulent flow. Moreover, the transition from laminar to turbulent flows will exert significant influences on

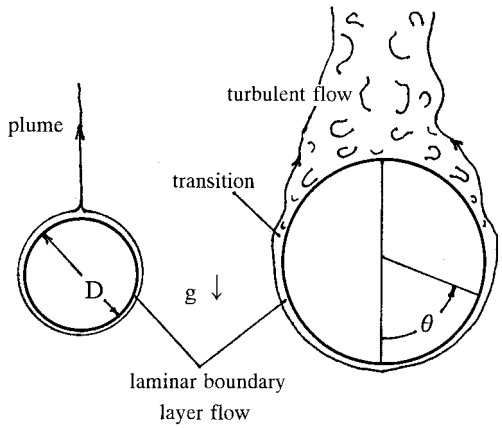

Fig. 1. Natural convection around cylinder.

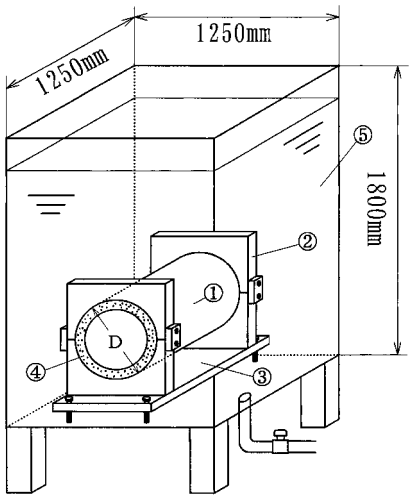

① Test Cylinder ② Side Plates ③ Base
④ Thermal Insulation ⑤ Water Tank

Fig. 2. Experimental apparatus.

the heat transfer from the cylinder. However, very little information has been available on the local heat transfer characteristics of large cylinders.

Taking account of the above circumstances, the authors started by conducting the intensive visualization experiments on the flow and temperature fields around cylinders to obtain comprehensive knowledge on the turbulent transition over heated cylinders. The flows over the cylinder and the surface temperatures of the cylinders were visualized using dye and liquid crystal thermometry, respectively. Water at room temperature was used as a test fluid and the test cylinders were heated with uniform heat fluxes for convenience of visualization and the heat transfer measurement. Secondly, local heat transfer coefficients were measured to investigate the correlation between flow fields and local heat transfer characteristics over cylinders. The diameter of the test cylinders was varied from 60 to 800 mm to perform the experiments in extremely wide ranges of the modified Rayleigh numbers from 3.0×10^8 to 3.6×10^{13}.

2. Experimental apparatus and measurements

The present experimental apparatus is schematically illustrated in Fig. 2. The apparatus consisted of a test cylinder, side plates, a base and a water tank. The test cylinder was fabricated with an acrylic resin pipe 4 mm thick and stainless steel foil heaters 30 μm thick. The heaters were glued on the outer surface of the cylinders and were connected in series. A uniform heat flux condition was realized by supplying AC power to the heaters. Water-repellent foam rubbers 20 mm thick thermally insulate the inner surface of the cylinder to reduce the conduction heat loss. Cylinders with the diameter 60, 95, 114, 165, 216, 300, 500 and 800 mm were prepared to enable the experiments in a wide range of modified Rayleigh numbers, while the length of the cylinder remained constant at 500 mm. For the simplicity of the flow configuration, high aspect ratios of the cylinders are preferable. However, the limitation in the size of water tank made it difficult to attain high aspect ratios for the 500 and 800 mm cylinders. Thus, side plates were attached on the both ends of the cylinders in order to inhibit incoming flows from the sides. The result was satisfactory. These plates have realized a two-dimensional flow configuration over the cylinders. This will be mentioned in the later section.

For the purpose of the heat transfer measurements, local surface temperatures of the heated cylinders, $T_{w\theta}$, were measured with Chromel–Alumel thermocouples of 100 μm diameter. They were spot-welded on the back of the heaters along the periphery of the cylinder with angular intervals of 2.5 to 5°. Thermocouples of the same material and diameter as above measured the temperatures of the ambient fluid, T_∞. They were placed 200 mm apart from the cylinder and with a vertical interval of 500 mm. Preliminary experiments on the heat transfer show that the conduction heat loss from the inner surface of the cylinders was less than 3% of the total heat generation on the heaters. Thus, the surface heat fluxes of the cylinder, q_w, were calculated from input electrical power to the heaters, Q, and total surface area of the cylinder, A, as: $q_w = Q/A$, by neglecting the heat loss. Using the above temperatures and the heat fluxes, the local heat transfer coefficients, h_θ, at angular location θ from the bottom were defined as: $h_\theta = q_w/(T_{w\theta} - T_\infty)$.

In order to minimize the influences of thermal prop-

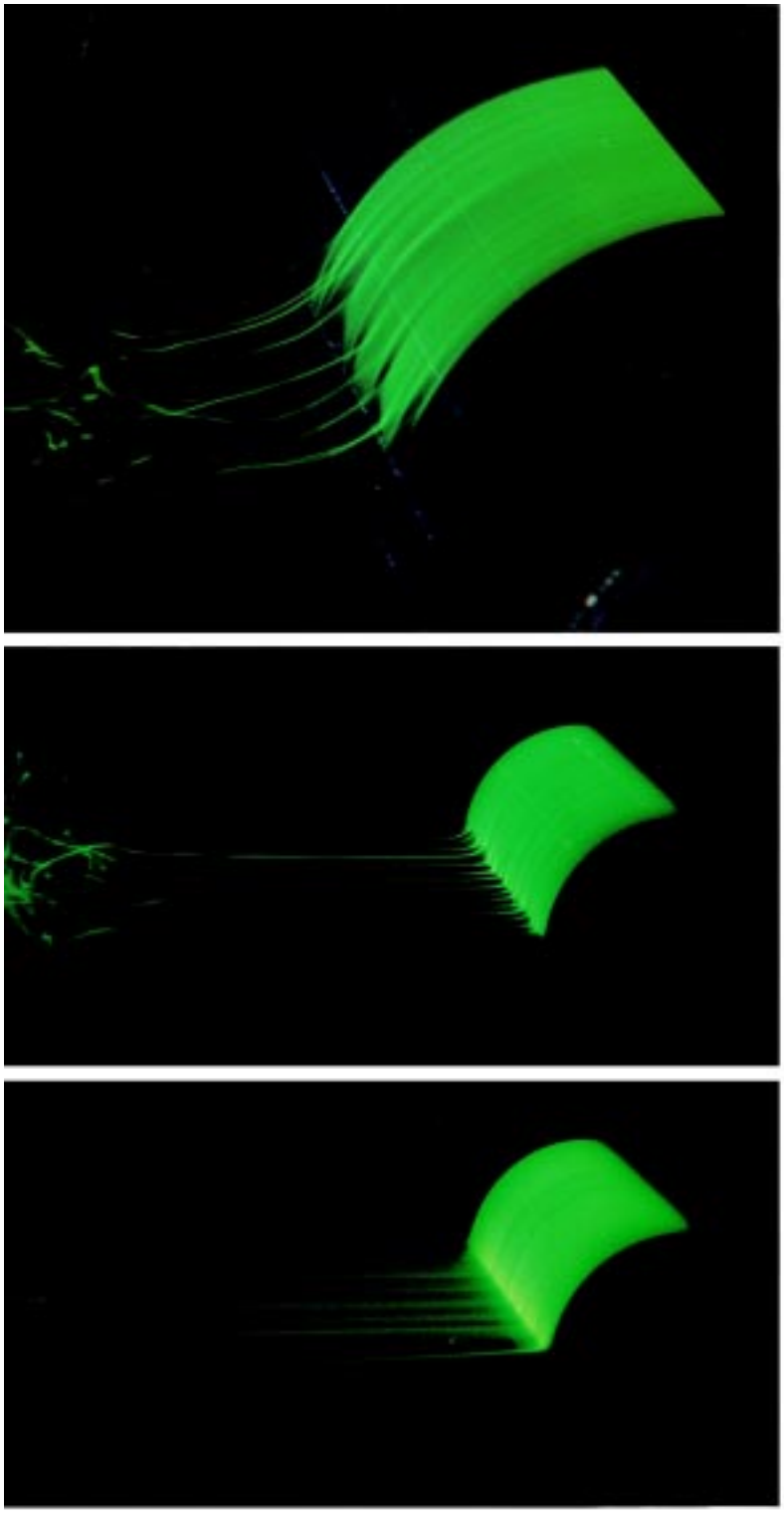

Fig. 3. Visualized flow fields around cylinders.

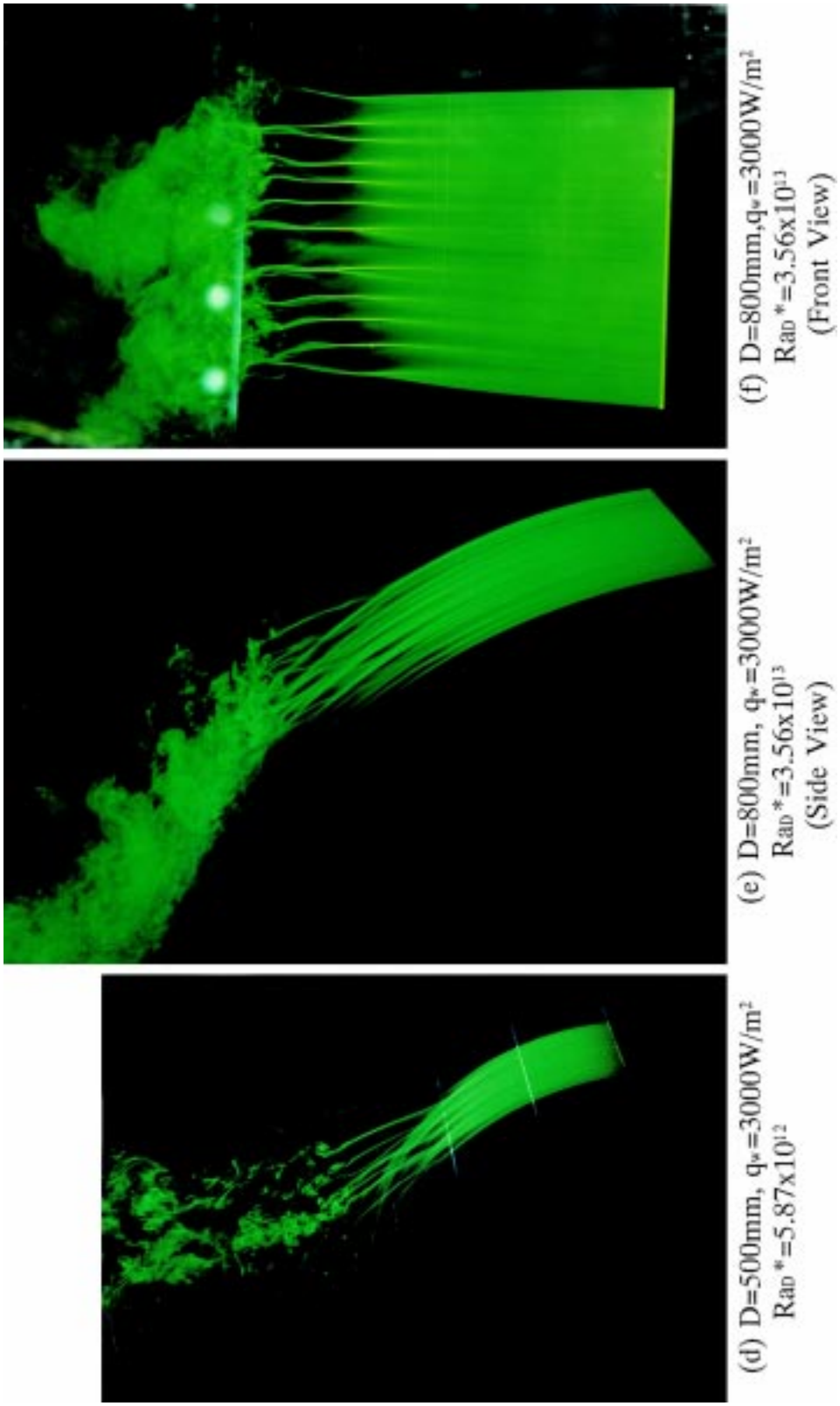

Fig. 3 (*continued*)

erty variations on the coefficients, the ambient temperature of the water was maintained at $20 \pm 1°C$, and also the temperature differences between the cylinder and ambient fluid were kept within 15 K throughout the experiments. Thermophysical properties in non-dimensional parameters were estimated at the film temperatures as: $T_f = (T_w + T_\infty)/2$.

The above test cylinder was fixed to the base and was placed horizontally on the bottom of rectangular water tank, 1250×1250 mm^2 cross-sectional area and 1800 mm deep. The bottom edge of the cylinder was located 300 mm above the horizontal base plate, and the screws attached on the base plate adjusted the level of the cylinder.

3. Results and discussions

3.1. Visualization of flow fields over cylinders

The flows adjacent to heated cylinders were visualized first with dye to obtain basic knowledge on the turbulent transition over cylinders. The typical results are given in Fig. 3. In order to visualize the flow field two-dimensionally, a long slit was installed at the bottom or side of the cylinders. Fig. 3(a) represents the flow field around a 95 mm cylinder. The dye issued from the slit first flows along the cylinder surface, subsequently detaches from the trailing edge of the cylinder, and finally ascends away as a laminar plume. Fig. 3 also depicts that a laminar boundary layer covers the whole surface of the cylinder. When the surface heat flux is increased to 3000 W/m^2, the dye ascending along the cylinder surface separates three-dimensionally from the trailing edge of the cylinder, and forks into many filaments as shown in Fig. 3(b). Similar separations are also observed over the cylinders of 300, 500 and 800 mm in diameter as shown in Fig. 3(c)–(e). The separation points shift sideward of the cylinder with the increase in diameter. Moreover, Fig. 3(e) demonstrates that the dye filaments after separation fluctuate irregularly, and a fully turbulent state is realized at certain distance from the separation. The turbulent flow still ascends along the surface and leaves from the top of the cylinder. Fig. 3(f) represents the front view of the dye streaks. The dye filaments just behind the separation appear with almost constant pitches in the axial direction. We also observed that these filaments are generated from the fixed points over the cylinder and these points remain stationary.

The above figures also reveal that the three-dimensional separation becomes a trigger to the turbulent transition. Thus, we investigated the three-dimensional separation further. One of the particular concerns is the condition of the three-dimensional separation at the trailing edge, because the condition will provide an onset condition for the turbulent transition. In order to determine this condition, the visualization experiments were performed with the cylinders of 60, 95 and 114 mm diameter and under various surface heat fluxes. The results showed that the three-dimensional separations occur when the modified Rayleigh numbers of the cylinders exceed 2.1×10^9.

The separation points shift from the trailing edge to the sides of the cylinders with further increase in the Rayleigh numbers. The separation points are another concern of the present study, because the flows over the cylinder can be classified into the upstream laminar flow and the downstream transitional and turbulent flows according to the separation points. Thus, we investigated the separation points under the various conditions of cylinder diameters and surface heat fluxes. It is, however, difficult to determine the separation points exactly because of the complexity of the three-dimensional separation, so that the locations where the dyes begin to detach from the cylinder surface were defined as the separation points. The separation points show variations in the spanwise direction, so that their average locations were measured in the present study. The results are given in Fig. 4, where the angles of separation points, θ, measured from the leading edge of the cylinder are plotted in terms of the modified Rayleigh numbers, Ra^*_D.

As is obvious from Fig. 4, the separation first appears at $\theta = 180°$ when $Ra^*_D = 2.1 \times 10^9$, and the separation points gradually shift sideward of the cylinder with the Rayleigh numbers. However, they remain at around $\theta = 120°$ even at the maximum Rayleigh number of the present experiments, $Ra^*_D = 3.6 \times 10^{13}$. The result, in turn, indicates that the transitional and turbulent regions occupy only 1/3 of the total surface area. The result is worth while noting, because the regions are far smaller than those expected by the previous workers.

Careful observations on Fig. 4 reveal that the separation points cannot be determined solely with the modified Rayleigh numbers, but they also depend on the cylinder diameters. In order to obtain a non-dimensional correlation that can predict the separation points more strictly, several arrangements were performed on the above data by using various non-dimensional parameters. However, the arrangements have failed. This is partly because of the following reason. The present separation takes place as a result of the thermal instability of the laminar boundary layer. While, many parameters, such as the cylinder diameter, surface heat flux, inclination angle of the surface, streamwise distance from the leading edge, will affect the above instability. Thus, it is difficult to deduce appropriate non-dimensional parameters from the combinations of these parameters. Besides, the present cylinders were heated with constant heat flux, so that

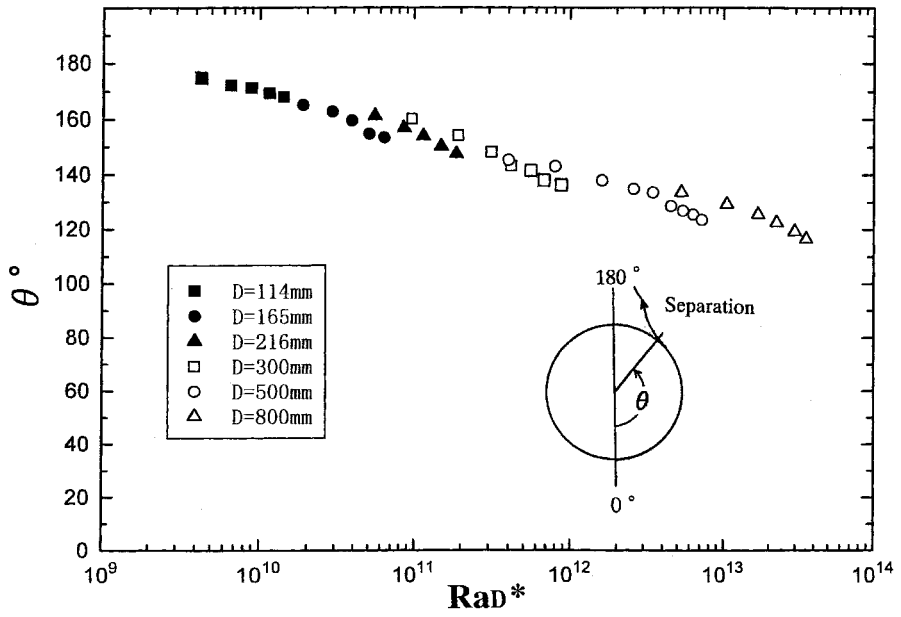

Fig. 4. Location of separation point.

the thermal properties of the fluid vary along the circumference of the cylinders. This also makes the exact arrangements difficult.

The next concerns were axial pitches of the three-dimensional separation. As was demonstrated in Fig. 3(f), the dye filaments just behind the separation appear at almost constant pitches. It is of physical importance to investigate the pitches of the dye filaments. Thus, the pitches were measured under the various conditions of the cylinder diameters and the surface heat fluxes, and the values were averaged to yield the mean axial pitches, P. In the present experimental

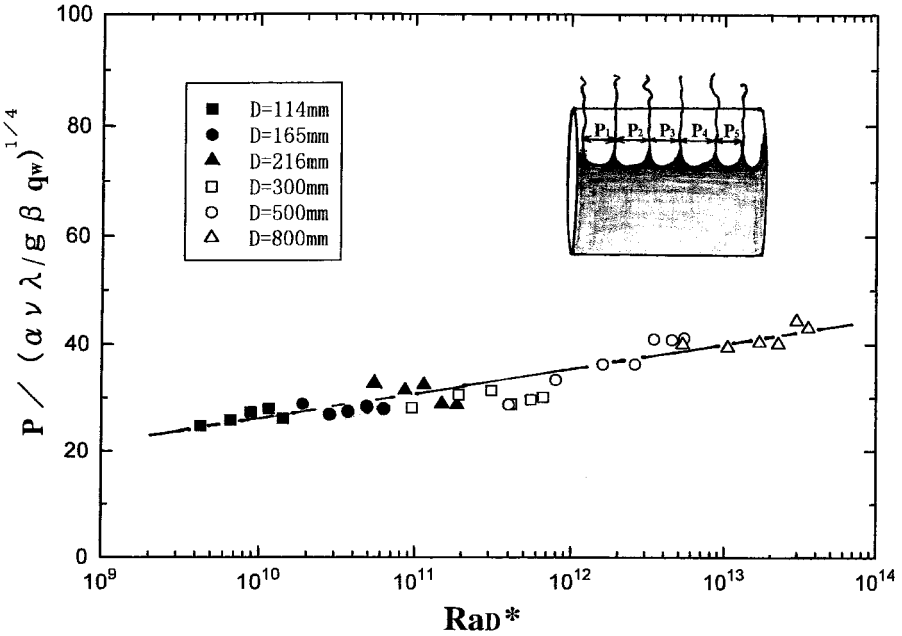

Fig. 5. Mean axial pitches of separation.

ranges, the mean axial pitches, P, vary from 8 to 21 mm, and they become larger with the diameter and smaller with the heat flux. The pitches normalized with the length scale, $le=(\alpha\nu\lambda/g\beta q_w)^{1/4}$, are plotted in terms of Ra_D^* and are shown in Fig. 5. Although thus normalized pitches increase slightly with the Rayleigh numbers, they are collected within the narrow band around the solid line shown in the figure.

3.2. Visualizations of surface temperatures

We proceed to visualize the surface temperatures of the test cylinders using liquid crystal thermometry. The experiments aim to obtain comprehensive knowledge not only on the temperature fields adjacent to the cylinders but also on the local heat transfer characteristics around the cylinders. Fig. 6 shows the typical

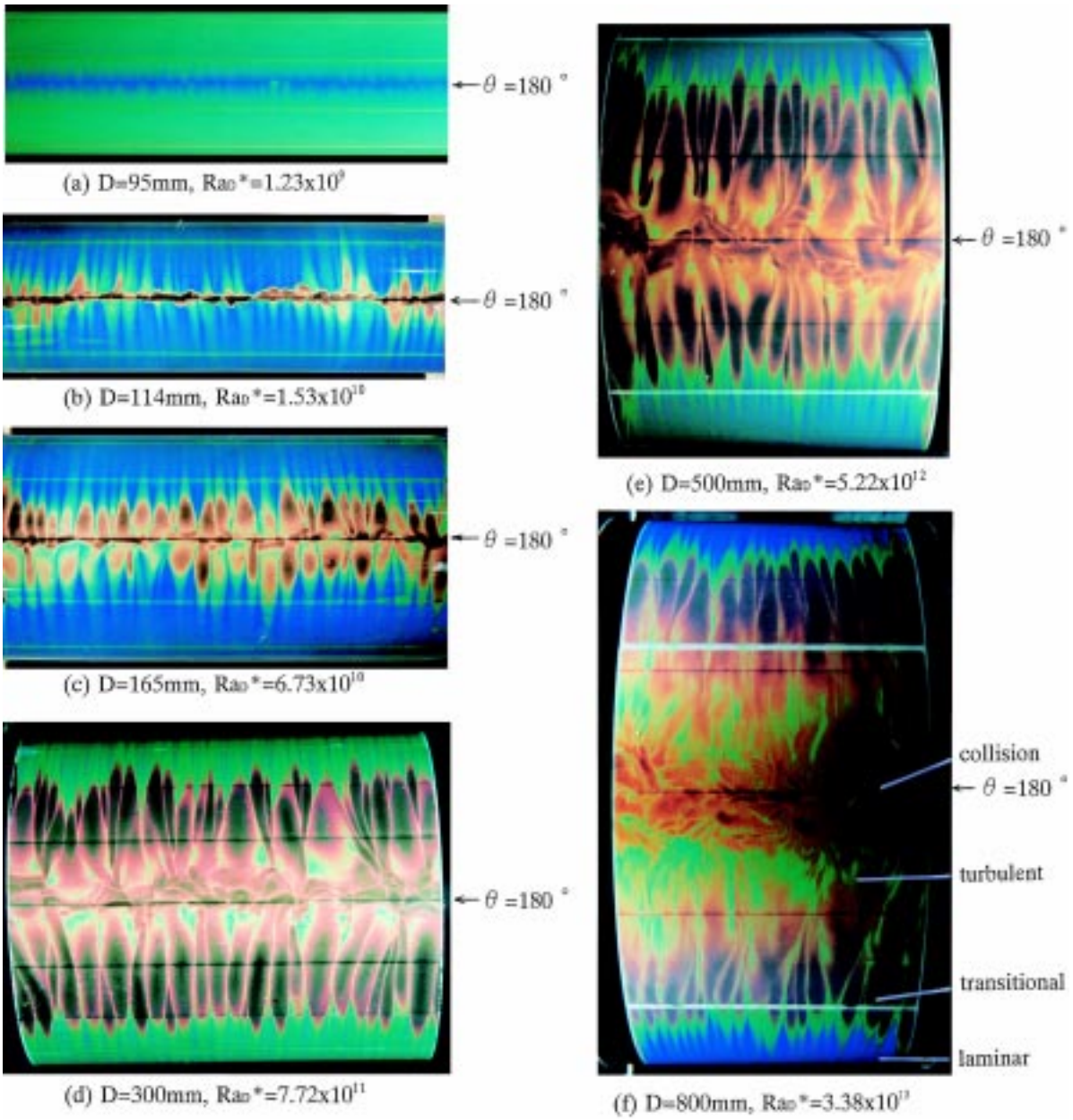

Fig. 6. Visualized surface temperatures of cylinders.

results for the cylinders with different diameters. These photos were taken from directly above the cylinders; thus, the horizontal centerlines of the photos correspond to the trailing edge of the cylinders. Before discussing the results, some explanations shall be added for the interpretation of these photos. The liquid crystal sheet utilized in the present experiments change color from dark red to blue with increasing temperatures. The yellow and green colors show intermediate temperatures. These photos also represent the distributions of the local heat transfer coefficients. Since the test cylinders were heated with uniform heat flux and the ambient water temperature was maintained constant, the regions of high (blue) and low (dark red or blown) temperatures represent the regions of the low and high heat transfer coefficients, respectively. We will also find several low-temperature, horizontal lines in those figures, but these lines merely show dividing lines of the heater strips.

Fig. 6(a) depicts the result for the 95 mm cylinder, of which Rayleigh number is less than the critical Rayleigh number, $Ra^*_{DC} = 2.1 \times 10^9$. The temperatures are uniform in the axial direction but show variation in the peripheral direction, with the highest temperatures appearing at the trailing edge of the cylinder. The result implies that the heat transfer coefficients decrease with the distance from the bottom and reach the minimum value at the top of the cylinder. Although similar variation in the surface temperatures is observed for the 114 mm cylinder, low-temperature spots appear near the trailing edge of the cylinder as shown in Fig. 6(b). These spots are elongated downward and become streaky with further increase in the cylinder diameter as are demonstrated in Fig. 6(c) and (d). The above streaks appear with almost constant axial pitches. Moreover, we observed that the heads of the streaks in Fig. 6(d) remain stationary, while their tails begin to fluctuate irregularly. Meanwhile, we conceive different temperature pattern, which is characterized by small and dense low-temperature pattern, appears near the trailing edge of 300 and 500 mm cylinders as shown in Fig. 6(d) and (e). The pattern moves randomly but sway around the top of the cylinder.

Moreover, another temperature pattern exists in between the streaky pattern and the pattern near the trailing edge as shown in Fig. 6(f). The pattern moves randomly and changes its shape at every moment. As a result, the following four temperature patterns are distinct on the surface of the 800 mm cylinder. These are: (i) two-dimensional pattern in the upstream region of the cylinder, (ii) steady and streaky pattern downstream of the pattern (i), (iii) unsteady and irregular pattern next to pattern (ii), and (iv) small and dense pattern near the top of the cylinder. Among these patterns, pattern (ii) is of particular importance, because the region occupies a considerable portion downstream of the separation. Therefore, further visualization experiments were carried out to investigate the reasons for the above pattern.

In Fig. 7, the flow field is visualized when the three-dimensional flow separation occurs over the cylinder. In addition to the dye from the slit, another dye is injected slowly from a small stainless-steel pipe placed 5 mm apart from the surface. The latter dye enters the pocket in between the dye filaments and reaches to the surface downstream of the separation. Since the dye injected from the pipe represents the movement of low-temperature ambient fluid, the attachment of the ambient fluid causes the low-temperature streaky patterns. This is confirmed by the combined visualization with dye and liquid crystal sheet. The combined visualizations also showed that the small and dense temperature patterns near the trailing edge are generated as a result of mixing and collision of flows ascending along both sides of the cylinders. Taking account of these facts, and also comparing the results shown in Figs. 3 and 6, the regions (i), (ii), (iii) and (iv) previously mentioned can be referred as the laminar, transitional, turbulent and collision regions, respectively.

It should be noted that similar temperature patterns as above have been observed in natural convection over horizontal, heated plates facing upward [6]. Fig. 8 shows a typical example of visualized surface temperatures of the plate heated with uniform heat flux. The

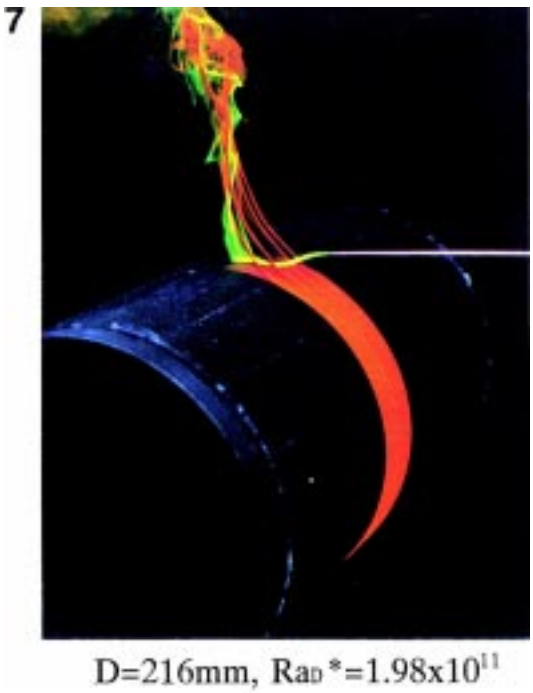

Fig. 7. Visualized flow field around cylinder.

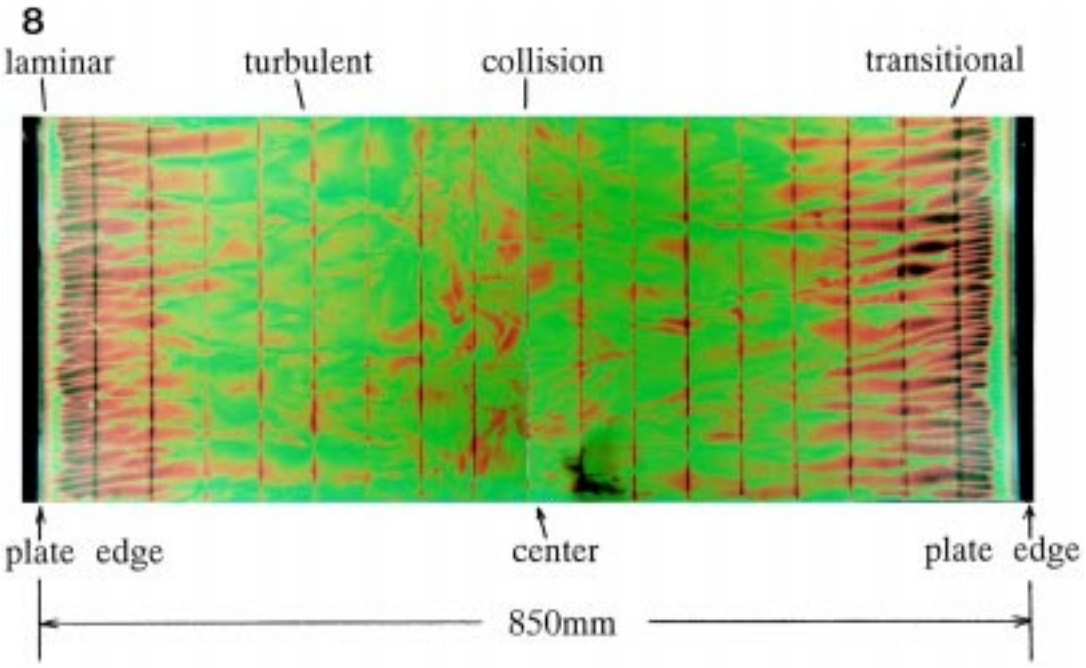

Fig. 8. Visualized surface temperature of upward-facing horizontal plate heated with constant heat flux.

photo was taken from directly above the plate when the plate was 850 mm wide. Although the slight differences in the size and extent of temperature patterns exist between those over the plate and those over an 800 mm cylinder, similarities in patterns from (i) to (iv) are obvious. The result suggests that the similar mechanisms of turbulent transition work both over a horizontal cylinder and a horizontal plate.

3.3. Local heat transfer coefficients

In light of the above results on the surface temperatures, we subsequently measured the local heat transfer coefficients using thermocouples. A problem arises as for the local heat transfer measurements in the transition region, because the low-temperature streaks appear in the region and their locations remain stationary. The occurrence of such streaks will lead to marked axial variations in the coefficients. Therefore, the coefficients from this region were defined as the values averaged in the axial direction. In spite of the definition, it was still difficult to determine the coefficients precisely from the output of the thermocouples, because the pitches of the streaks were of the order of several to twenty millimeters and we could not place thermocouples at intervals small enough to detect the axial variations.

Meanwhile, we observed that these streaks change their location during a run conducted under the same experimental conditions. Making use of this fact, we repeated the measurements of the surface temperatures at least 20–30 times while keeping the same experimental conditions. The thermocouples were placed symmetrically with respect to the vertical centerline of the cylinder, so that over 40–60 data were collected to yield the local heat transfer coefficients. An error analysis was also performed on these data. The results indicate that the above numbers are large enough for the calculation of the mean values. The maximum deviation of the calculated coefficients against the real coefficients is estimated to be less than $\pm 5\%$ at 95% coverage.

The typical results of the local heat transfer coefficients thus obtained are given in Fig. 9 with the case of constant heat flux, $q_w = 2000$ W/m^2, and of variable cylinder diameters. The local Nusselt numbers divided by 1/5 power of the modified Rayleigh numbers, $Nu_\theta / Ra_D^{*1/5}$, are plotted in terms of the angles from the bottom, θ.

The local Nusselt numbers for the 60 mm cylinder show monotonous decrease with the angles. This is attributable to the development of laminar boundary layer over the cylinder. Since the modified Rayleigh number of this cylinder is less than the critical Rayleigh number, $Ra_D^* = 2.1 \times 10^9$, the laminar boundary layer flow cover the whole surface. Similar variations in the local Nusselt numbers are also observed in the bottom and side regions of 95 and 114 mm cylinders. However, the Nusselt numbers of the 114 mm cylinder depart from the above laminar plots

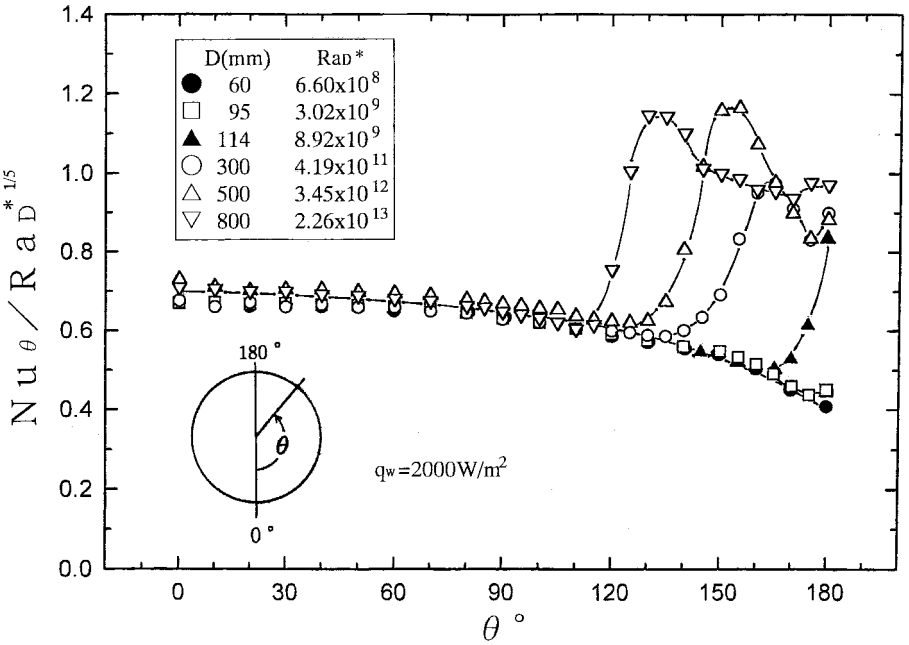

Fig. 9. Local Nusselt numbers of cylinders.

and increase rapidly at the angle beyond 170°. The regions of the increased Nusselt numbers gradually expand upstream as the diameter increases. In particular, the local Nusselt numbers of the 800 mm cylinder show marked increase from $\theta = 110°$, and reach a maximum at around $\theta = 130°$. In the downstream of the maximum, they turn to decrease and show almost constant values at $\theta = 140$–$165°$, then, increase slightly toward the trailing edge of the cylinder.

Comparing these results with those of the flow and temperature visualizations, the following relations were found to exist between the local heat transfer and the flow and temperature fields. Those are: (1) minimum Nusselt numbers appear just upstream of the separation, (2) the marked increase in the local Nusselt numbers occur in the transitional region, and (3) the almost constant Nusselt numbers are realized in the turbulent region. It is worth while noting that the turbulent region occupies only a small portion of the surface even over the 800 mm cylinder, and also that the region can hardly appear over the cylinders smaller than 500 mm in diameter.

3.4. Average heat transfer coefficients

Based on the local Nusselt numbers obtained in the above, we calculated the average Nusselt numbers of the cylinders, Nu_m. The results are plotted in terms of the modified Rayleigh numbers, Ra^*_D, and are shown in Fig. 10. As was mentioned in Section 1, several workers have proposed the correlation equations for the average Nusselt numbers. These equations are applicable to both the laminar and turbulent heat transfer. For comparison, the equations proposed by McAdams [1], Morgan [2] and Churchill and Chu [3] are represented with the lines in the figure. In order to compare the present results for the uniform heat flux cylinders with the previous equations for the isothermal cylinders, the latter equations are transformed using the relation $Ra^*_D = Ra_D Nu_D$. Then, the equations are expressed as follows:

McAdams [1];

$$Nu_m = 0.597 Ra_D^{*1/5} \quad (\text{where } 5.3 \times 10^4 < Ra^*_D < 9.3 \times 10^{10}) \tag{2}$$

$$Nu_m = 0.215 Ra_D^{*1/4} \quad (\text{where } 1.3 \times 10^{11} < Ra^*_D < 1.3 \times 10^{15}) \tag{3}$$

Morgan [2];

$$Nu_m = 0.556 Ra_D^{*1/5} \quad (\text{where } 4.8 \times 10^4 < Ra^*_D < 2.7 \times 10^8) \tag{4}$$

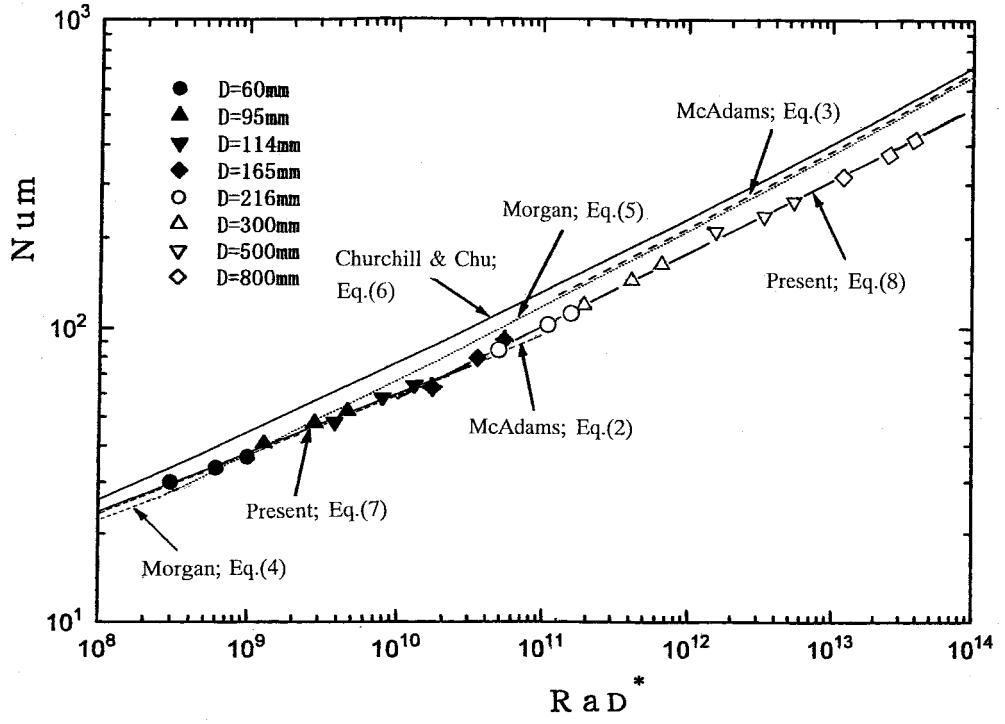

Fig. 10. Average Nusselt numbers of cylinders.

$$Nu_m = 0.210 Ra_D^{*1/4} \quad \text{(where } 2.7 \times 10^8 < Ra_D^* < 1.3 \times 10^{15}\text{)} \tag{5}$$

Churchill and Chu [3];

$$Nu_m^{1/2} = 0.60 + 0.361 (Ra_D^*/Nu_m)^{1/6} \tag{6}$$

On the derivation of Eq. (6), $Pr = 6$ is assumed in their original equation for simplicity and the value corresponds to the present experimental Pr number. Eq. (6) is applicable to both laminar and turbulent flows.

As is obvious from Fig. 10, the present Nusselt numbers show different dependencies in the regions of the modified Rayleigh numbers; $Ra_D^* < 2.5 \times 10^{10}$ and $Ra_D^* > 2.5 \times 10^{10}$, and they can be correlated with the following two equations:

$$Nu_m = 0.6 Ra_D^{*0.2} \quad \text{(where } 3.0 \times 10^8 < Ra_D^* < 2.5 \times 10^{10}\text{)} \tag{7}$$

$$Nu_m = 0.23 Ra_D^{*0.24} \quad \text{(where } 2.5 \times 10^{10} < Ra_D^* < 3.6 \times 10^{13}\text{)} \tag{8}$$

Based on the previous definition and also on the above result, the present critical Rayleigh number for the turbulent transition may become as $Ra_{DC}^* = 2.5 \times 10^{10}$. However, it should be recalled that the actual transition occurs at smaller Rayleigh number, $Ra_{DC}^* = 2.1 \times 10^9$, as was revealed by the present visualizations. The above discrepancy in the critical Rayleigh numbers can be explained as follows. Although the local Nusselt numbers are increased markedly in the transitional and turbulent regions, these regions occupy only a small portion to the total cylinder surface and the heat transfer is determined mainly by the laminar convection. Thus, the average Nusselt numbers remain almost the same as the laminar values even if the Rayleigh numbers exceed the critical value. Taking account of the above fact, the critical Rayleigh numbers determined from the overall heat transfer seem inaccurate.

We next compare the present results with the previous empirical equations. As shown in Fig. 10, present data coincide fairly well with McAdams' laminar correlation, Eq. (2), in the region of smaller Rayleigh numbers, $3 \times 10^8 < Ra_D^* < 2.5 \times 10^{10}$. While in the higher Rayleigh number region, $2.5 \times 10^{10} < Ra_D^* < 3.6 \times 10^{13}$, present results show at around 15% smaller Nusselt numbers than those esti-

mated from Eqs. (3), (5) and (6). Although exact reasons for this discrepancy are uncertain at present, one of the possible reasons will be due to the Prandtl numbers of the test fluid. The previous equations have been derived mainly from the experimental results with air, while the present data were obtained with water. The difference in the Prandtl number may cause the above discrepancy. The second possible reason is attributable to the previous correlation equations. Some of the previous workers have derived the equations by averaging the existing experimental data obtained by others. However, the data show considerable scatters between the workers, so that a simple average of the data may cause the deviations against the real Nusselt numbers. To assure the above reasons, further experiments particularly using air as a test fluid will be needed.

4. Conclusions

The fluid flow and heat transfer of natural convection around large horizontal cylinders were investigated experimentally in the present study. Special concerns were the high-Rayleigh-number flows that undergo the turbulent transition. In order to investigate the conditions of turbulent transition and also the transition mechanisms, the flow over the cylinders and the surface temperatures of the cylinders were visualized with dye and liquid crystal thermometry, respectively. The measurements of local heat transfer coefficients were subsequently carried out to investigate the relation between the visualized flow fields and the local heat transfer characteristics. Test fluid was water at room temperature. The cylinders were heated with uniform heat fluxes. The diameter of the cylinders ranged from 60 to 800 mm and this enabled the experiments in wide ranges of modified Rayleigh numbers from 3×10^8 to 3.6×10^{13}. The results are summarized as follows:

1. The flow visualizations with dye revealed the following phenomena appear over the cylinders when the Rayleigh numbers are high enough. (i) Laminar boundary layer develops over the cylinder from the leading edge to the separation point. (ii) The boundary layer, then, separates three-dimensionally from the surface. (iii) Transitional flow appears downstream of the separation. (iv) The flow after separation fluctuates irregularly and becomes turbulent. (v) The turbulent flows ascending along the both sides of the cylinder merge with each other near the trailing edge and ascend away from the cylinder as a turbulent plume.
2. The above results suggest that the three-dimensional separation becomes a trigger to the turbulent transition. The separation first appears at the top of the cylinders when $Ra^*_D = 2.1 \times 10^9$. If the Rayleigh number is less than the above, the flow remains laminar throughout the circumference of the cylinder. While, if the Rayleigh number exceeds the above critical number, three-dimensional separation takes place over the cylinder. The separation points shift upstream of the cylinder with further increases in the modified Rayleigh number.
3. The surface temperature visualizations with liquid crystal sheets demonstrated that the following four distinct temperature patterns appear over the cylinders according to the distance from the bottom of the cylinder. These are; (vi) the two-dimensional temperature patterns upstream of the separation, (vii) the steady and streaky low-temperature patterns behind the separation, (viii) the unsteady and irregular low-temperature patterns downstream of (vii), and (ix) the dense and irregular temperature patterns near the top of the cylinder. The comparisons of these results with those of the flow visualizations showed that the above regions (vi), (vii), (viii) and (ix) correspond to the laminar, transitional, turbulent and collision regions, respectively.
4. Similar flow and temperature fields mentioned in the above have been observed in the natural convection over horizontal, heated plates facing upward. The result suggests that the turbulent transitions over horizontal cylinders undergo similar mechanisms as those over horizontal, heated plates.
5. The local heat transfer coefficients from the cylinders were also measured with the thermocouples. It was revealed that the coefficients were increased significantly in the transitional and turbulent regions. Based on these data, correlation equations for the average Nusselt numbers were proposed. The present equation for the region of the Rayleigh numbers, $2.5 \times 10^{10} < Ra^*_D < 3.6 \times 10^{13}$, gives 15% smaller Nusselt numbers than those estimated from the previous empirical equations.

References

[1] W.H. McAdams, Heat Transmission, 3rd ed., McGraw-Hill, New York, 1954, pp. 175–177.
[2] V.T. Morgan, The overall convective heat transfer from smooth circular cylinders, in: T.F. Irvine Jr, J.P. Hartnett (Eds.), Advances in Heat Transfer, vol. 11, Academic Press, New York, 1975, pp. 199–210.
[3] S.W. Churchill, H.S. Chu, Correlation equations for laminar and turbulent free convection from a horizontal cylinder, Int. J. Heat Mass Transfer 18 (1974) 1049–1053.
[4] B. Farouk, S.I. Guceri, Natural convection from a hori-

zontal cylinder—turbulent regime, Trans. ASME, J. Heat Transfer 104 (1982) 228–235.

[5] Y. Hattori, Turbulent natural convection boundary layer around horizontal cylinder, Proceedings of National Heat Transf. Conference of Japan (special issue), Heat Transfer Society of Japan (in Japanese) 33 (1996) 853–854.

[6] K. Kitamura, F. Kimura, Heat transfer and fluid flow of natural convection adjacent to upward-facing horizontal plates, Int. J. Heat Mass Transfer 38 (1995) 3149–3159.